P. D. Anderson, D. Ternet, G. W. M. Peters, H. E. H. Meijer*

Materials Technology, Dutch Polymer Institute, Eindhoven University of Technology, Eindhoven, The Netherlands

Experimental/Numerical Analysis of Chaotic Advection in a Three-dimensional Cavity Flow

Advection of material volumes in a three-dimensional cavity flow is analyzed by using an experimental setup and a collection of computational tools. The experimental setup for the lid-driven cavity flow makes it possible to study the advection of drops for a wide range of flow parameters. The location of unmixed regions for a specific mixing protocol is predicted by means of the mapping method, which are then used to determine the initial location of the dyed drops in the experiments. Finally, an adaptive front tracking method is used to computationally follow the drops during flow in a precise way. In most cases, a qualitative comparison between the experiments and the simulations is found. In addition, the mapping method proves to be well suited to quickly predict unmixed regions in mixers.

1 Introduction

The two-dimensional lid-driven cavity flow is one of the most used prototype flows to study the fundamentals of laminar mixing in drag flows, both theoretically and experimentally [1 to 5]. However, most of these studies are limited to Newtonian fluids (exception are for example the papers [5 to 7]). This is a severe limitation considering the practice of mixing where mostly viscoelastic fluids (polymers, food, etc.) are involved. Experiments with (highly) viscoelastic fluids in a two-dimensional, open lid-driven cavity flow are troublesome because normal stresses will cause the free surface to deform considerably, making a two-dimensional flow impossible, demanding a closed flow cell. Also, extending the two-dimensional cavity mixing flow to three-dimensional requires a new experimental setup. In conclusion, studying experimentally the fundamentals of the mixing behavior in three-dimensional, both for Newtonian and viscoelastic fluids, requires a confined geometry.

The analysis of laminar mixing of passive fluids (i. e. no influence of interfacial tension) in three-dimensional flows started with the paper of *Feingold* [8], and was followed by several numerical studies [9 to 12] studying all types of different phenomena occurring in three-dimensional flows. Experimental work has focused on chaotic mixing in three-dimensional flows in pipes [13], and major advances in the area of visualization of these three-dimensional flows are achieved by the work of *Kusch* [14], who studied chaotic advection in some continuous flows. *Khakhar* and *Ottino* [15] analyzed one of these systems, the partitioned pipe mixer (PPM), in more detail. It consists of a rotating pipe and inside of it a series of flat partitions at right angles to each other. These experimental studies clearly show regular structures and chaotic mixing in a three-dimensional flow. More recently, *Fountain* et al. [12] studied mixing in a cylindrical tank with a flat disk impeller, where to achieve chaotic behavior the impeller angle was made adjustable. Other efforts are reported in [16 to 19].

Our goal is to study experimentally mixing in a three-dimensional mixing cavity, a prototype flow for more complicated industrial mixing problems, and to compare the experimental results with those from a numerical approach. Previous theoretical research has resulted in different methods to study the complex flow fields and mixing performance in confined mixing geometries. In special cases the location and nature of periodic points in the flow can be determined [11]. Periodic points are defined as points in a time periodic flow in which the fluid returns to its original position after one or more periods of the flow. The nature of these periodic points can be either elliptic or hyperbolic depending on the deformation that the fluid experiences throughout the period. Material around elliptic points undergo a simple rotation while those around hyperbolic points are contracted in one direction and stretched in the other. As a result, regions around elliptic points (called islands) undergo rather poor mixing while material approaching hyperbolic points is mixed in a very efficient way.

An effective approach to study distributive mixing is the use of the mapping method, which was proposed in *Kruijt* et al. [20] and related to ideas of *Spencer* and *Wiley* [21]. The main idea is not to track each material volume in the flow domain separately, but to create a discretized mapping from a reference grid to a deformed grid. Instead of tracking the boundaries of material volumes a set of distribution matrices is used to advect a concentration field or other properties.

This mapping technique has been compared to more rigorous tracking methods and shown to accurately reproduce the results. In addition, it allows the calculation of mixing efficiencies, for a given mixing protocol, in minutes computational time rather than hours, like needed for tracking [22]. Up to now these mapping simulations have yet to be verified with experiments and that is the one of the purposes of this work. We also want to demonstrate the feasibility of such an experiential

* Mail address: P. D. Anderson, Materials technology, Dutch Polymer Institute, Eindhoven University of Technology, P.O. Box 513, 5600 MB Eindhoven, the Netherlands
E-mail: p.d.anderson@tue.nl

set up and, therefore, in this paper we restrict ourselves to Newtonian flow of passive fluids. Here, we present the experimental setup used to study the flow in a three-dimensional mixing cavity and the results of a study in which we compare the mixing for drops placed near an elliptic point and around a hyperbolic point. With this work, we seek to confirm the predictions for a relatively simple system (creeping flow, Newtonian drops, no surface tension) before tackling more complicated flows and fluids in future studies.

2 Experimental Setup

The three-dimensional mixing cavity consists of a $5 \times 5 \times 5$ cm cube made of PMMA with two opposite open sides, see Fig. 1 for an image of the setup and Fig. 2 for a schematic picture of the mixing cube. The cube contains a drain on the bottom face connected to a short length of Tygon tubing. Filling of the cube is done through the opened hatch on the top face and partly with the use of a syringe connected to the tubing on the drain at the bottom face. On the right side face of the cube a mirror is attached (and also one on the top side, but this is not used in the rest of this paper) so that next to front view side also a side view of the cavity may be obtained with a camera. The cube fits into a supporting stand between the two glass walls, which form the front and back faces of the cavity. Each wall is held in place by a two-frame setup that prevents leakage and allows translation of the walls in both vertical and horizontal directions. Each frame contains a stepper motor connected to a worm drive, which controls the motion of the wall or frame in one direction.

The four stepper motors which drive the motion of the walls are driven by BLHX Brushless Servo Drives by Digiplan. These drives are relayed together and are controlled by text commands from the computer through an RS-232 serial communications port. The light sources for this experiment are high-frequency fluorescent lamps mounted at the rear, bottom, and side of the mixing cavity. To diffuse the light, a screen has been mounted just a few centimeters in front of each of the lamps. The bottom lamp is rarely used in the existing setup, since the top view is too obstructed to give a clear view the drop.

To eliminate the effect of perspective in both the front and side views of the cavity, a telecentric (Carl Zeiss, VISIONMES 225/11/0,1) is used with the following properties: measuring field/object size = 184.5×184.5 mm, measuring accuracy = ± 8 µm, object to image distance = 720 mm, imaging scale = 1 : 20.45, depth of field = ± 90 mm. Video capture is accomplished with the use of a Kodak Megaplus Camera model ES 1.0 in conjunction with a Matrox Pulsar framegrabber board within the computer. All control of the experimental setup is done with a custom-written software application entitled three-dimensional Mixing Cavity Application. This software allows the user control of motor movement, camera properties, frame capture, video recording, calibration, and conversion of videos to AVI files or full frame images.

We used glycerol as the matrix fluid for its high viscosity, i. e. to limit the Reynolds number so a Stokes flow is obtained. The procedure used to create dyed glycerol blobs is relatively simple. 100 ml of Glycerol 99 + % (Aldrich Cat. No.: 13,487-2) is combined with roughly 0.030 grams of the Alphanol Fast Navy Blue R 200-PW (Hoechst DB MG 505) dye. The dye is added to the flask along with a stirrer bar, and the dye is stirred until the dye has completely dissolved in the glycerol. As the top surface of the glycerol makes contact with the top face of the cavity, the injection rate should be slow so that the number of bubbles created at the top face is minimized. With some persistence, it is possible to remove all the bubbles from the cavity. The percentage of dye used here has been arrived at after testing many different samples and optimizing for the best contrast between dyed and pure glycerol, especially for highly stretched drops, while still maintaining more or less neutral buoyancy. After creating a new dyed solution, it is checked that the properties, viscosity and density, of the dyed solution and the pure solution are identical. The simulations assume that the drop and surrounding fluid have identical viscosities (if not, then the simulations cannot be expected to match the experiments). Also, if the densities are not matched, the drop will either rise or sink during the course of the experiment. For the results shown in this paper the dyed solution and the pure glycerol so-

Fig. 1. The three-dimensional mixing cavity made of PMMA; clearly visible are the side and top mirrors

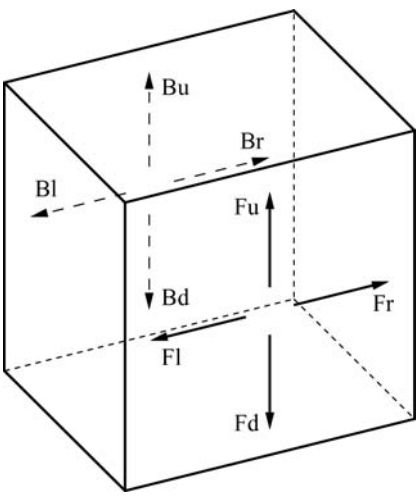

Fig. 2. Schematic picture of the three-dimensional mixing cavity

lution have identical viscosities of 1.0 Pa s and identical densities of 1.260 g/ml.

3 Problem Definition; Theoretical Setting; Numerical Methods

3.1 Tracer Kinetics

The motion of passive tracers is governed by the three-dimensional kinematic equation which describes the evolution of the positions $\mathbf{x}$ of tracers, initially positioned at the position $\mathbf{x}_0$ in the flow field $\mathbf{u}(\mathbf{x}, t)$:

$$\frac{d\mathbf{x}}{dt} = \mathbf{u}(\mathbf{x}, t), \qquad \mathbf{x}(0) = \mathbf{x_0}. \tag{1}$$

The solution of this dynamical system defines the map $\mathbf{x}(t) = \Phi_t(\mathbf{x}_0)$ and uniquely determines the positions $\mathbf{x}$ for any given initial tracer $\mathbf{x}_0$. In this paper only time-periodic mixing protocols are considered, thus $\mathbf{u}(x, t + T) = \mathbf{u}(x, t)$ with T the global period. This leads to the reduction of the continuous flow $\mathbf{x}(t) = \Phi_t(\mathbf{x}_0)$ into the discrete mapping Φ_T. The velocity field is described by the mass and momentum balance equations with appropriate boundary conditions as decribed in the following paragraph.

3.2 Flow Field

Since we restrict our analysis to quasi-steady incompressible Newtonian flow, the balance equations of mass and momentum read:

$$\mathbf{u} \cdot \nabla \mathbf{u} = -\nabla p + \frac{1}{Re} \nabla^2 \mathbf{u},$$

$$\nabla \cdot \mathbf{u} = 0, \tag{2}$$

where the velocity is represented by $\mathbf{u}$ and the pressure by p. Re denotes the Reynolds numbers yielding the ratio of inertia and viscous forces. The cube has dimensions $|x| \leq W$, $|y| \leq W, |z| \leq W$.

For stationary walls of the three-dimensional cubic cavity as shown in Fig. 2, homogeneous Dirichlet boundary conditions are imposed, while the condition $u = 1$, $v = 0$, $w = 0$ is applied for the moving front wall. The numerical solution of Eqs. 2 for the three-dimensional flow problems is performed by a projection scheme that decouples the pressure p and velocity $\mathbf{u}$ [23]. A spectral element approximation [24, 25] is used for the spatial discretization and yields an accurate representation of the velocity field. The cavity is subdivided into $15 \times 15 \times 15$ spectral elements, each of sixth order in all three directions, leading to 753,571 nodal points and a total system with 2,868,477 degrees of freedom. The resulting system of equations is solved using a conjugate gradient solver with a finite element preconditioner.

For creeping flow the fluid deformation caused by the wall movement is completely defined by the dimensionless displacement of the wall D, defined here as the wall displacement divided by the half of the cavity edge width 2W (which equals 1 in dimensionless coordinates). The relatively simple geometry forms a convenient model for testing the techniques designed to study three-dimensional laminar time-periodic distributive mixing. Due to symmetry properties of the flow, the velocity field has to be computed only for one type of the wall motion (in this case $\mathbf{F_r}$). The velocity fields for other wall motions can be obtained using a simple coordinate transformations.

3.3 Flow Configuration

The mixing protocol used in this paper consists of four steps and is denoted as

$$\mathbf{P} = \mathbf{B_d F_l B_u F_r}\,, \tag{3}$$

where the rightmost operator is acting first. The subscripts r, l, u, and d denote right, left, up, and down wall motions, respectively.

The symmetry operators $\mathbf{S}_x$, $\mathbf{S}_y$ and $\mathbf{S}_{xz}$ can be introduced:

$$\mathbf{S}_x(x, y, z) = (-x, y, z), \tag{4}$$

$$\mathbf{S}_y(x, y, z) = (x, -y, z), \tag{5}$$

$$\mathbf{S}_{xz}(x, y, z) = (z, y, x). \tag{6}$$

In addition the operator $\tilde{\mathbf{S}} = \mathbf{S}_y \mathbf{S}_{xz}$ is defined as:

$$\tilde{\mathbf{S}}(x, y, z) = (z, -y, x),$$

$$\tilde{\mathbf{S}} = \mathbf{S}_y \mathbf{S}_{xz} = \mathbf{S}_{xz} \mathbf{S}_y. \tag{7}$$

This operator, in fact, describes a rotation by 180°, i. e. axial symmetry, around the line defined by $y = 0,\ x - z = 0$. It is obvious that $\tilde{\mathbf{S}}\tilde{\mathbf{S}} = \mathbf{1}$ and, thus, $\tilde{\mathbf{S}}^{-1} = \tilde{\mathbf{S}}$, where $\mathbf{1}$ is the identity operator.

In [26] it is proven that the protocol $\mathbf{P}$ and its inverse $\mathbf{P}^{-1}$ posses the following symmetry relations:

$$\mathbf{P}^{-1} = \tilde{\mathbf{S}}\, \mathbf{P} \tilde{\mathbf{S}}, \qquad \mathbf{P} = \tilde{\mathbf{S}}\, \mathbf{P}^{-1} \tilde{\mathbf{S}}. \tag{8}$$

In terms of definitions as used *Franjione* [27] (and references therein) it means that the map $\mathbf{P}$ has a *time-reversal* symmetry $\tilde{\mathbf{S}}$. The same symmetry holds for the maps $\mathbf{P}^n$ for $n > 1$ [26]:

$$\mathbf{P}^{-n} = \tilde{\mathbf{S}}\, \mathbf{P}^n \tilde{\mathbf{S}} \quad \text{and} \quad \mathbf{P}^n = \tilde{\mathbf{S}}\, \mathbf{P}^{-n} \tilde{\mathbf{S}}. \tag{9}$$

The relations (9) and reversibility of the Stokes flow gives the possibility to reveal the symmetry that periodic structures of the flow under study must necessarily possess. Namely, periodic structures of any order (or the isolated points, if any) should be arranged symmetrically around the axis $y = 0$, $x - z = 0$. As an example to show that this protocol is able to yield chaotic advection of material volumes in Fig. 3 the deformation of a blob is shown. The numerical method which has been used to describe the advection is introduced in the following section. Clearly, the blobs undergoes a large deformation during flow and the repetitive process of stretching and folding is observed. Within these seven and a half periods of flow an exponential increase of interfacial area is observed. The initial spherical drop is described with 512 triangles using 258 nodes, while deformed structure after 7.5 periods contains 896,610 elements and 448,307 nodes. The increase of interfacial area is after these 7.5 periods equals 455 (!). These results are in-

cluded to demonstrate that with chaotic mixing in a short time material is advected throughout the flow domain and although extremely complex structures result they still can be accurately described. This exponential behavior observed here is also revealed in the experimental results shown later.

3.4 Adaptive Front Tracking

To study distributive mixing in the three-dimensional cavity flow it is necessary to track strongly deforming material volumes. As their deformation can be large, even up to exponential stretching, appropriate computational models are needed to follow the deformation. In this work the surface of a material volume is described by an unstructured triangular mesh, as done by *Unverdi* and *Tryggvason* [28 to 30]. Additional to their techniques, surface curvature is used here to decide about necessary mesh refinements. Local mesh refinement provides the possibility to use small elements in strongly curved zones of the surface (near sharp edges, for example), and much larger elements in relatively planar zones, keeping the number of elements as low as possible. This significantly reduces the amount of computational work needed to follow the material volumes. Also the pre-history of the surface deformation is used for adding new markers during mesh refinement. New markers are added on a less deformed, earlier configuration of the surface and then tracked to their current position.

As the mesh can become significantly distorted during flow, it should be refined where necessary. The most important part of the mesh refinement is contained in the choice of the criteria that define whether cells should be refined. The mesh refinement algorithm proposed here is controlled by three parameters:

- h_{max} – the maximum cell edge length.
- $h_{max,c}$ – the maximum length of an edge of a cell adjacent to an angle sharper than α_{max}.
- α_{max} – the critical angle between cells. The angle between neighbouring cells is defined as the angle between their outer normals.

Thus, the refinement algorithm takes into account the curvature of the surface, so that strongly curved parts of the surface are covered by small cells while relatively flat zones of the surface are described by large cells. This minimizes the number of markers and, thus, the computational expenses.

A master-slave scheme with dynamical workload distribution over slave processes in a PVM-network [31] is used as a parallel algorithm to speedup the adaptive front tracking and its efficiency can be found in *Galaktionov* et al. [32].

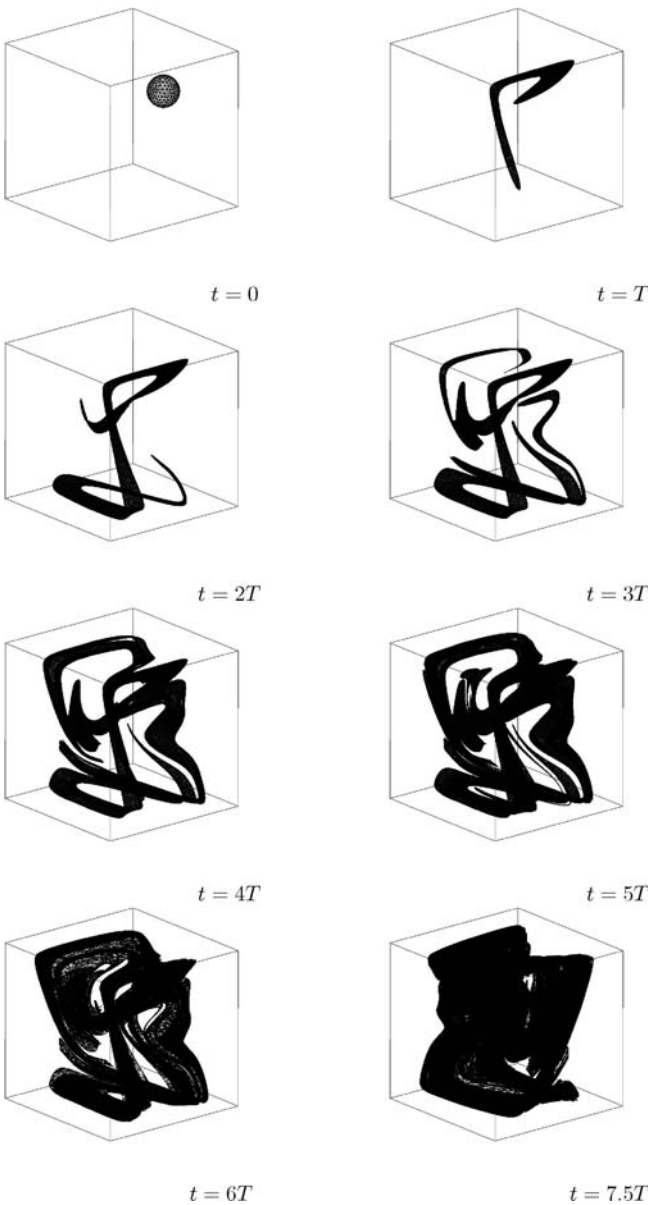

Fig. 3. Advection of a material blob in the three-dimensional cavity flow using protocol P and D = 3

4 Results

We present experimental results for a single mixing protocol showing the comparison to the tracking simulations for drops placed near an elliptic point and near a hyperbolic point, using mixing protocol applied is $\mathbf{P} = \mathbf{B_d F_l B_u F_r}$ (see Fig. 2 for definitions); so first the front wall moves to the right, next the back wall up, the front wall to the left and finally the back wall moves down. Note that after this period that the walls have all returned to their original location allowing the use of the (finite) glass plates. With the internal cube size as length scale, the dimensionless displacement equals D = 3, with a corresponding wall velocity of 8 mm/s. With the viscosity and density of the glycerol solution, the Reynolds number, Re, for this flow is 0.5.

4.1 Determining Unmixed Regions

Before starting the experiments and selecting the initial location of the drops inserted, we applied the mapping method to analyze the chosen mixing protocol. The mapping technique

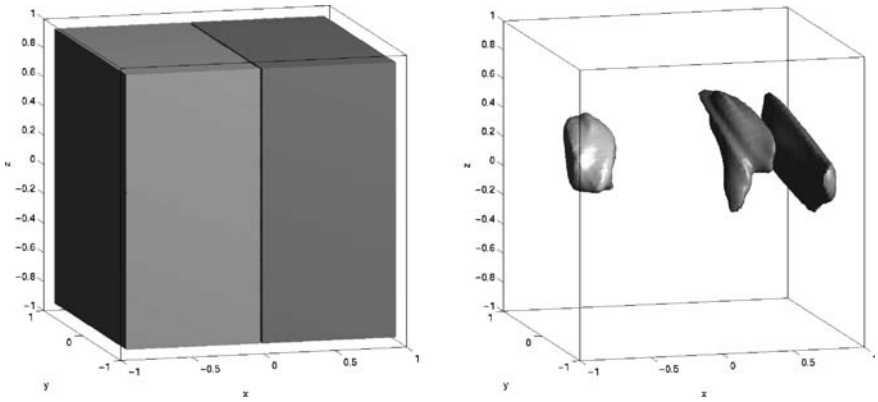

Fig. 4. Initial distribution 1 and detected unmixed zones

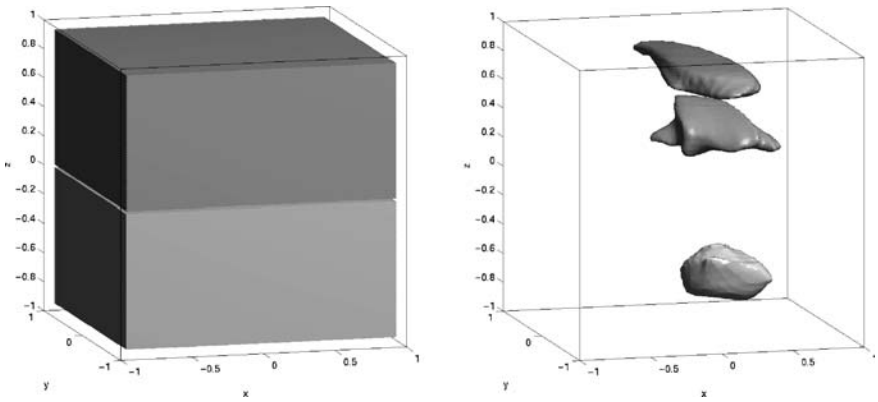

Fig. 5. Initial distribution 2 and detected unmixed zones

has proven to be an efficient method to compare and optimize different mixers and mixing protocols. For different two-dimensional flows optimal mixing parameters were determined [20, 33], but also in three-dimensional efforts are made to look at industrial mixers. Results are published for three-dimensional mixing in a confined geometry, i. e. the cavity flow [22], in static mixers like the Kenics mixer [34], the multiflux [35] and the SMX mixer [36], but also in dynamic mixers like a twin screw extruder [37].

Less known is that the mapping method can also be used to determine unmixed regions, called islands, in the mixer in a simple way. The idea is straightforward. If we start to mix and an island is initially completely filled with one polymer (say $c = 0$), then that component will always remain in the island. On the other hand, outside the island the components mix and we observe a transition from the single polymer to the mixed composition. If we determine the iso-surfaces, $c = 0$ and $c = 1$, during mixing, and compare them after each period, the unmixed region is easily detected.

Unfortunately, if the island is initially filled with both components, observing the unmixed regions is not so obvious since, in an island, linear mixing occurs making it impossible to detect the iso-surfaces $c = 0$ and $c = 1$. To overcome this drawback we use to following simple strategy: different distributions of initially placed concentration fields possibly yield different groups of unmixed regions. If the different regions are assembled into a single figure we get an overview of the unmixed areas in the mixer. Of course, this approach provides no guarantee that all islands are found. One might even argue that for sure not all islands are located, simply by the fact that some islands might be very small, much smaller than the resolution used for the grid in the mapping method. Most likely, the tiny islands around high-order elliptic points will be undetected. If

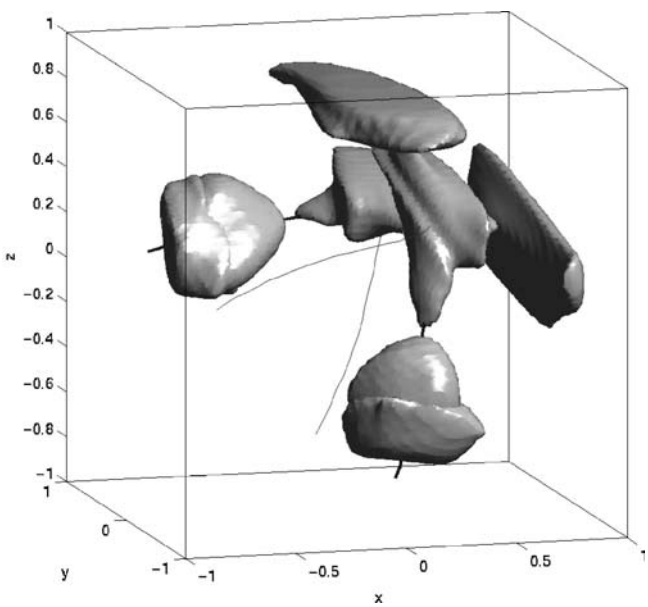

Fig. 6. Islands collected using different initial distributions

one is interested in locating these, of course a more refined mapping grid can be used or one could create a high-resolution Poincaŕe map. To the authors knowledge, determining all islands in bounded three-dimensional flows has not received much attention in the literature. In this paper, we limit ourselves to the larger islands associated with low-order elliptic periodic points.

The left plot in Fig. 4 shows the case where the cavity is initially vertically divided by two components and on the right the isosurfaces for c = 0 and c = 1 are shown after ten periods of mixing for D = 3. In this case we observe three islands. Another set of islands is found by choosing a horizontal division of the two components. The plot on the right of Fig. 5 shows the isosurfaces found now. Other combinations of an initial distribution of the two fluids did not lead to additional, not earlier detected, unmixed regions.

Fig. 6 shows the combined plot where both sets of unmixed regions are collected in a single images. The islands are superimposed on the periodic lines found earlier for this mixing flow, see *Anderson* et al. [11] for more information on this subject.

4.2 Experiments versus Simulations

The collection of unmixed regions as shown in Fig. 6 is used as an initial guidance to choose the initial position of the drops. We start by showing the results for a drop placed near where we expect to find an elliptic point from the mapping analysis and thus expect to see very little stretching.

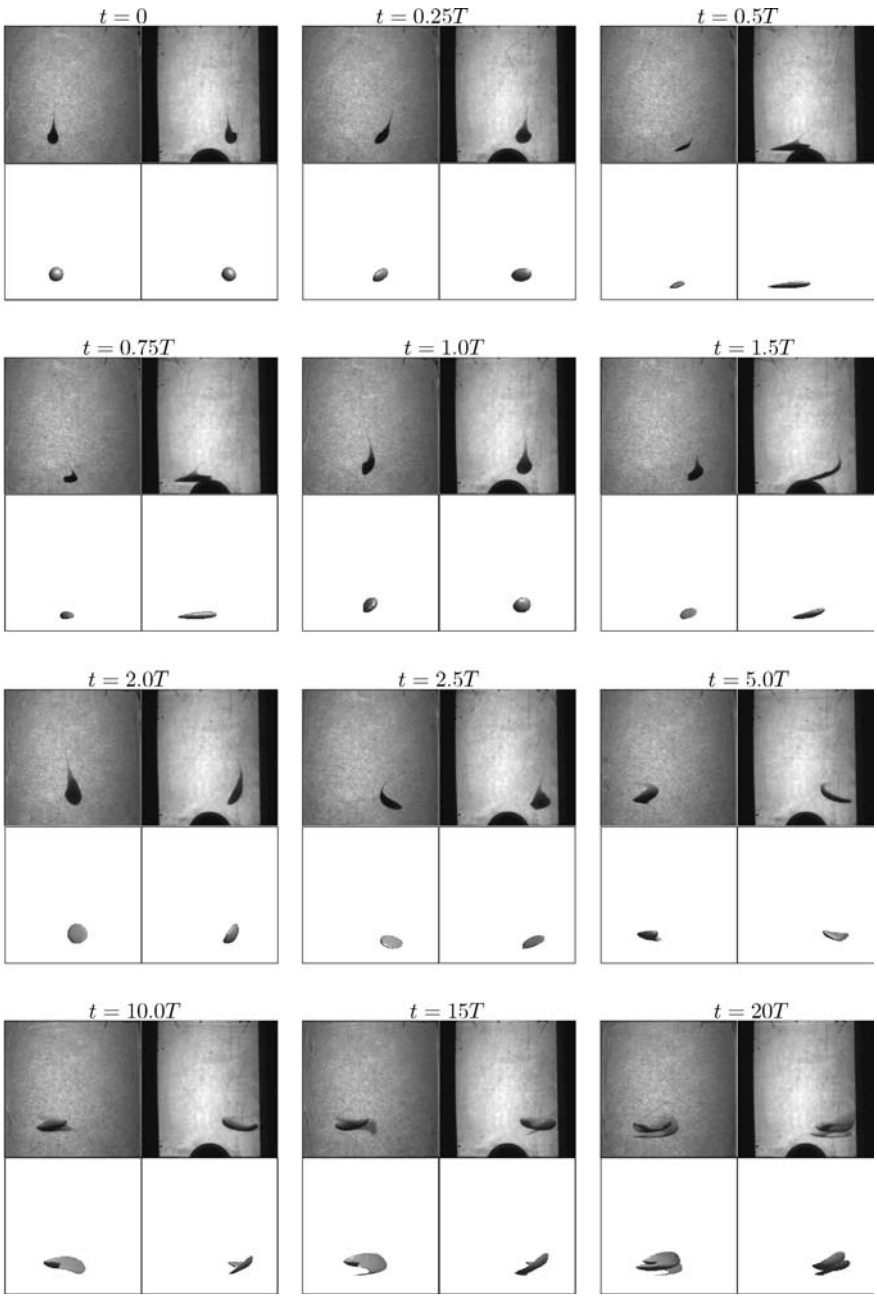

Fig. 7. Advection of a drop (x, y, z) = (−0.291, 0.313, −0.633) with radius 0.102 for t = 0 till t = 20T. Top images are experiments, bottom images are front tracking results

In Fig. 7 the initial position of the drop was $(x, y, z) = (-0.291, 0.313, -0.633)$, while the drop radius R was 0.102 where all values are in scaled coordinates. The results are shown in a series of images where the upper pair of images represent the experimental images of the front and side views of the mixing cavity, while the lower pair of images are the results of the front tracking simulations for the front and side views, see Figs. 7 and 8. The parameters used in the front tracking scheme are:

$$h_{max} = 0.5R, \qquad h_{c,max} = 0.2R.$$

From Figs. 7 and 8, it is easy to see the very close match between the experiments and simulations. A small deviation may be attributed to the fact that the original drop was not precisely spherical and the initial condition of the simulation is. By applying advanced three-dimensional image analysis tools one could determine a more proper description of the initial drop in the experiments and use that as an input for the simulations. In this work, however, we did not pursue this direction.

Next a drop is placed close to a hyperbolic point so we expect to see a large amount of stretching. The location of the initial drop was $(x, y, z) = (-0.316, 0.025, 0.004)$, while the drop radius was 0.207. For this particular drop the shape of the drop was far from spherical and, therefore, the initial condition used for the simulations was the smallest sphere that would include the entire blob in the first image of the series. As a result, we anticipate that as the experimental drop deforms, it should stay within the drop deformation predicted in the simulation.

In Figs. 9 and 10, one can see the nice resemblance between the simulations and the experimental frames out to 20 periods. Further comparisons are made difficult due to the a-spherical nature of the initial drop. Moreover, we would expect for drops placed far away from elliptic points, where there is a great deal of stretching taking place, that comparisons with the simulations will always be difficult since a small error in the size and placement of the initial drop can quickly lead to a significant deviation in the simulated drop shapes over 20 periods.

Finally, we have chosen one last case that illustrates the difficulties that can occur in obtaining quantitative comparisons

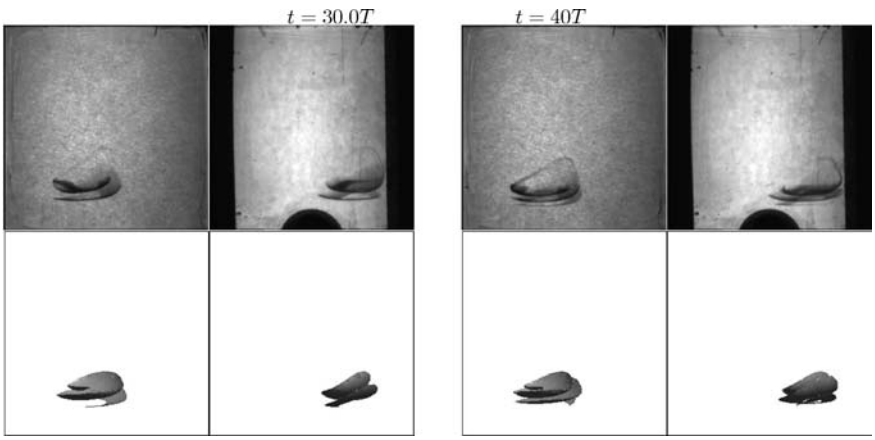

Fig. 8. Advection of a drop initially located at (x, y, z) = (−0.291, 0.313, −0.633) with radius 0.102 for t = 30T and t = 40T. Top images are experiments, bottom images are front tracking results

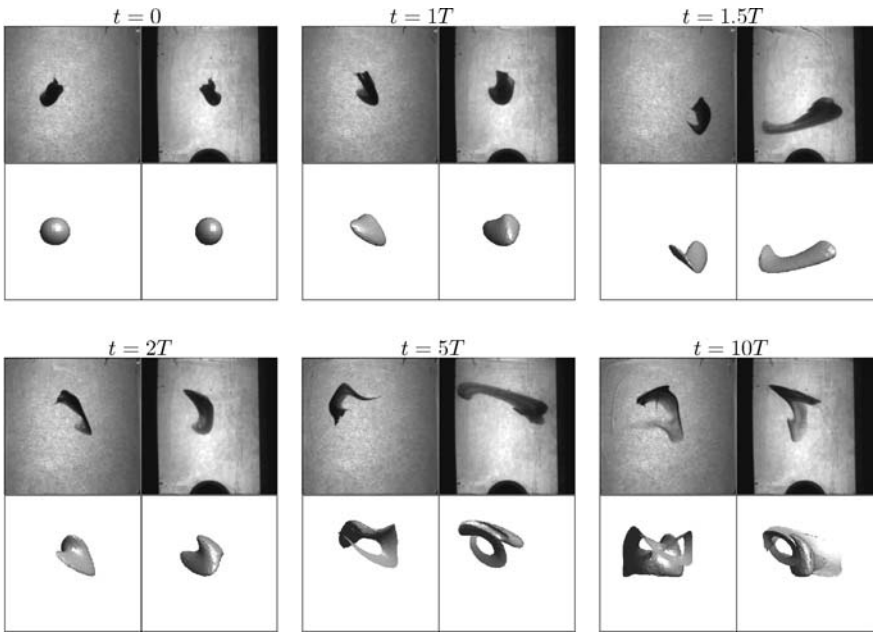

Fig. 9. Advection of a drop (x, y, z) = (−0.316, 0.025, 0.004) with radius 0.207 for t = 0 till t = 17.5T

for highly stretched drops, see Fig. 11. For this series, the location of the initial drop was (x, y, z) = (0.018, 0.545, −0.24), while the drop radius was 0.12. The drop was reasonably spherical to begin the experiment and so we did not expect that to be a significant contributor to the deviation. A few selected frames are shown in Fig. 11.

In this case, the simulation and experimental frames closely match up until around 5 periods, at which point the experimental images show the beginning of very large deformation. The drop then seems to form a figure eighth shape in the experimental images, while the simulations show similar shapes in only the bottom half with none of the upper portion of the deformed drop appearing at all. A part of the discrepancy may be due to the tail that extended from the initial drop in the experiments, which may have contributed, to the upper portion of this figure eight shape.

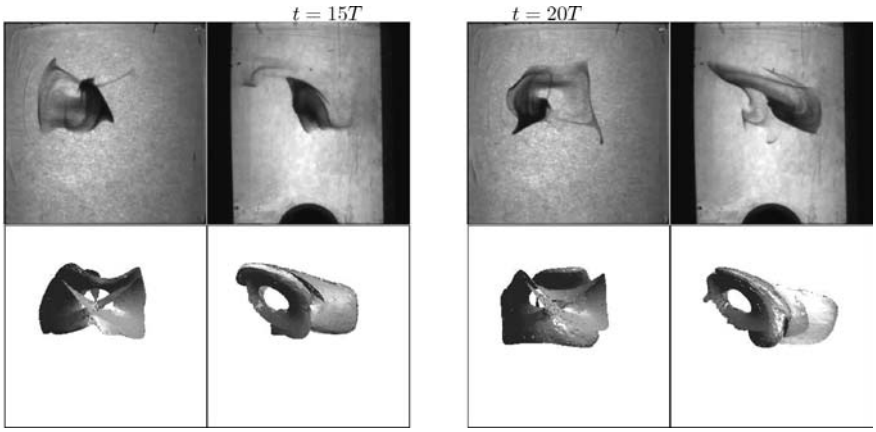

Fig. 10. Advection of a drop (x, y, z) = (−0.316, 0.025, 0.004) with radius 0.207 for t = 15T and t = 20T

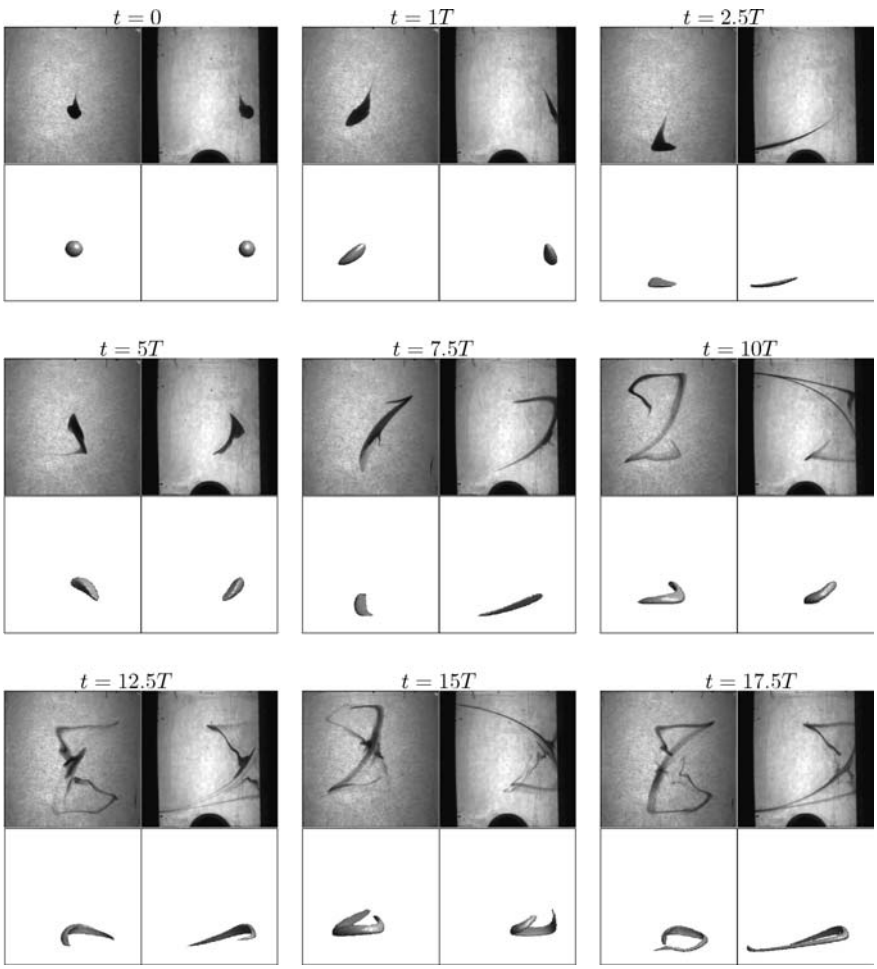

Fig. 11. Advection of a drop (x, y, z) = (0.018, 0.545, −0.24) with radius 0.120 for t = 15T and t = 20T

5 Conclusions

Overall, the simulations agree quite well with the experiments and for slightly deforming drops a case could be made for a quantitative comparison even out to 20 periods. In the cases where the drops have been shown to deform much more, the agreement is partly qualitative in nature with some regions appearing in the simulations not showing up in the experimental images, and vice versa. Some of the disagreement can be attributed to the difficulty in obtaining a perfectly spherical drop as an initial condition for the experiments. Also, for drops with large deformations, a small error in the position and/or size of the initial drop could lead to significantly different deformations after only a few periods of mixing.

As already mentioned in our introduction, studying experimentally the fundamentals of mixing in three-dimensional flows with viscoelastic fluids requires a confined geometry. Free surfaces in a viscoelastic flow will in general deform leading to secondary flows. In this paper it is shown that, within limitations, the setup can be used to study chaotic mixing. Placing a drop near an elliptic point within a sufficiently large island (i. e. larger than the drop) provides a procedure where the hardly deforming drop can be tracked over many periods rather well. This result is not related with the constitutive behavior (Newtonian or viscoelastic) of the matrix material. Therefore, this setup is considered to be suited to study experimentally more complicated systems, i. e. active fluids and viscoelastic fluids, in order to validate numerical models of such mixing flows.

References

1 *Chien, W. L., Rising, H., Ottino, J. M.:* J. Fluid Mech. 170, p. 355 (1986)
2 *Ling, F. H., Schmidt, G.:* Phys. Lett. A 165, p. 221 (1992)
3 *Meleshko, V. V., Peters, G. W. M.:* Phys. Lett. A 216, p. 87 (1996).
4 *Anderson, P. D., Galaktionov, O. S., Peters, G. W. M., van de Vosse, F. N., Meijer, H. E. H.:* Int. J. Heat & Fluid Flow 21, p. 176 (2000)
5 *Anderson, P. D., Galaktionov, O. S., Peters, G. W. M., van de Vosse, F. N., Meijer, H. E. H.:* J. Non-Newtonian Fluid Mech. 93, p. 265 (2000)
6 *Leong, C. W., Ottino, J. M.:* Phys. Rev. Letters 64, p. 874 (1990)
7 *Fan, Y., Tanner, R. I., Phan-Thien, N.:* J. Fluid Mech. 412, p. 197 (2000)
8 *Feingold, M., Kadanoff, L. P., Piro, O.:* J. Statist. Phys. 50, p. 529 (1988)
9 *Bajer, K., Mofatt, H. K.:* J. Fluid Mech. 212, p. 337 (1990)
10 *Ashwin, P., King, G. P.:* J. Fluid Mech. 285, p. 215 (1995)
11 *Anderson, P. D., Galaktionov, O. S., Peters, G. W. M., v. d. Vosse, F. N., Meijer, H. E. H.:* J. Fluid Mech. 386, p. 149 (1999)
12 *Fountain, G. O., Khakhar, D. V., Mezic, I., Ottino, J. M.:* J. Fluid Mech. 417, p. 265 (2000)
13 *Peerhossaini, H., Castelain, C., Leguer, Y.:* Expl. Termal Fluid Sci. 7, p. 33 (1993)
14 *Kusch, H. A., Ottino, J. M.:* J. Fluid Mech. 236, p. 319 (1992)
15 *Khakhar, D. V., Franjione, J. G., Ottino, J. M.:* Chem. Engng. Sci. 42, p. 2909 (1987)
16 *Hobbs, D. M., Muzzio, F. J.:* Phys. Fluids 10(8), p. 1942 (1998)
17 *Liu, S., Hrymak, A. N., Wood, P. E.:* Laminar flow in an SMX static mixer. Chem. Engng. Sci. 2005 (in press)
18 *Zalc, J. M., Szalai, E. S., Muzzio, F. E., Jaffer, S.:* AIChE J. 48, p. 427 (2002)
19 *Speetjens, M. F. M., Clercx, H. J. H., van Heijst, G. J. F.:* J. Fluid Mech. 514, p. 77 (2004)
20 *Kruijt, P. G. M., Galaktionov, O. S., Anderson, P. D., Peters, G. W. M., Meijer, H. E. H.:* AIChE J. 47, p. 1005 (2001)
21 *Spencer, R. S., Wiley, R. H.:* J. Colloid Sci. 6, p. 133 (1951)
22 *Galaktionov, O. S., Anderson, P. D., Kruijt, P. G. M., Peters, G. W. M., Meijer, H. E. H.:* Comput. Fluids 30, p. 271 (2001)
23 *Timmermans, L. J. P., Minev, P. D., van de Vosse, F. N.:* Int. J. Num. Meth. Fluids 22, p. 673 (1996)
24 *Anderson, P. D.:* PhD thesis, Eindhoven University of Technology, Eindhoven, The Netherlands (1999)
25 *Maday, Y., Patera, A. T.:* Spectral element methods for the incompressible Navier–Stokes equations. In: *Noor, A.* (Ed.), ASME, New York (1989)
26 *Galaktionov, O. S., Anderson, P. D., Peters, G. W. M.:* Phys. Fluids 12, p. 469 (2000)
27 *Franjione, J. G., Leong, C.-W., Ottino, J. M.:* Phys. Fluids. A 1, p. 1772, November (1989)
28 *Tryggvason, G., Unverdi, S. O.:* Phys. Fluids A 5, p. 656 (1990)
29 *Unverdi, S. O., Tryggvason, G.:* Phys. Fluids D 60, p. 70 (1992)
30 *Unverdi, S. O., Tryggvason, G.:* J. Comput. Phys. 100, p. 25 (1992)
31 *Geist, A., Beguelin, A., Dongarra, J., Jiang, W., Manchek, R., Sunderman, V.:* Parallel Virtual Machine. A user's guide and tutorial for networked parallel computing. The MIT Press, Cambridge, Massachusetts (1994)
32 *Galaktionov, A. S., Anderson, P. D., Peters, G. W. M.:* Mixing simulations: tracking strongly deforming fluid volumes in 3D flows. In: *Bubak, M., Dongarra, J., Wasniniewski, J.* (Eds.), Vol. 1332 of Lecture Notes in Computer Science, p. 463, Springer (1997)
33 *Anderson, P. D., Galaktionov, O. S., Peters, G. W. M., Meijer, H. E. H., Tucker III, C. L.:* Int. J. Numer. Meth. Fluids 40, p. 345 (2002)
34 *Galaktionov, O. S., Anderson, P. D., Peters, G. W. M., Meijer, H. E. H.:* CJChE Journal 80, p. 604 (2002)
35 *Kruijt, P. G. M., Galaktionov, O. S., Peters, G. W. M., Meijer, H. E. H.:* Int. Polym. Process. XVI, p. 151 (2001)
36 *Galaktionov, O. S.:* PhD thesis, Eindhoven University of Technology, Eindhoven, The Netherlands (2002)
37 *Kruijt, P. G. M., Galaktionov, O. S., Peters, G. W. M., Meijer, H. E. H.:* Int. Polym. Process. XVI, p. 161 (2001)

Acknowledgements

Financial support for this work was provided by the Dutch Polymer Institute (# 161).

Date recieved: November 2, 2005
Date accepted: January 25, 2006